



## CHARACTERIZATION OF NONLINEAR OPTICAL ABSORPTION AND REFRACTION

E. W. Van Stryland, M. Sheik-Bahae, A. A. Said and D. J. Hagan

Center for Research in Electro-Optics and Lasers, University of Central Florida,  
Orlando, FL 32826, U.S.A.

We discuss the characterization of nonlinear optical processes that give rise to changes in the absorption coefficient and refractive index. We primarily concentrate on methods for determining the dominant nonlinearities present in condensed matter and the responsible physical mechanisms. In extensive studies of a wide variety of material, we have found that there is seldom a single nonlinear process occurring. Often several processes occur simultaneously, sometimes in unison, sometimes competing. It is necessary to experimentally distinguish and separate these processes in order to understand and model the interaction. There are a variety of methods and techniques for determining the nonlinear optical response, each with its own weaknesses and advantages. In general, it is advisable to use as many complementary techniques as possible over a broad spectral range in order to unambiguously determine the active nonlinearities. Here we concentrate on the use of nonlinear transmittance, Z-scan and degenerate four-wave mixing experiments as applied to polycrystalline and single crystal semiconductors and dielectric materials.

### 1. Introduction

Numerous techniques are known for measurements of nonlinear refraction (NLR) and nonlinear absorption (NLA) in condensed matter. As the names imply, NLR describes optically induced changes in the refractive index of a material, while optically induced changes in absorption are categorized as NLA. Nonlinear interferometry [1,2], degenerate four-wave mixing (DFWM) [3], nearly-degenerate three-wave mixing [4], ellipse rotation [5], beam distortion, [6,7] beam deflection [8], and third-harmonic generation [9], are among the techniques frequently reported for direct or indirect determination of NLR. Z-scan is a single beam technique for measuring the sign and magnitude of NLR indices and NLA coefficients [10,11], which offers simplicity as well as high

sensitivity. Other techniques for measuring NLA include transmittance [12], calorimetry [13], photoacoustic [14], and excite-probe [15] methods.

Despite the wide range of available methods, it is rare that any single experiment will completely determine the physical processes behind the nonlinear response of a given material. The most important point to be made in this paper is that a single measurement of the nonlinear response of a material, at a single wavelength, and a single pulsewidth may give very little information on the material. In general such a measurement should not be used to judge the device performance of a material or to compare one material to another. We will elaborate on this point by using data for semiconductors (eg. ZnSe) and dielectric materials (eg. BaF<sub>2</sub>). The importance of the pulsewidth and wavelength dependence of the nonlinear response will be demonstrated through these examples. We begin with a background description of the consequences of NLA and NLR in section II. Section III is divided into three subsections covering the experimental techniques of transmittance, Z-scan and DFWM. Each subsection gives a description of the experimental technique and experimental results along with the physical interpretation for the example materials. Section IV describes the importance of determining and understanding the frequency dependence of the nonlinearities and section V contains brief conclusions.

## II. Background

Nonlinear absorption directly affects the amplitude of the propagating electric field while NLR directly affects the phase. However, during propagation, phase changes propagate to give spatial (and temporal) amplitude changes. This can be seen as the coupling of phase and amplitude in the differential equation describing this propagation (i.e. the wave equation). A great simplification results by making the "thin sample approximation". In this approximation we can separate the wave equation into an equation for the phase  $\phi$ , and an equation for the irradiance,  $I$ , as a function of the depth  $z$  within the sample. We write the electric field as  $E = A\sqrt{I/n} \text{Re}[e^{i\phi} e^{i(kz-\omega t)}]$  where  $k$  is the wave number and  $A$  is a material independent constant of proportionality. The thin sample approximation allows us to separate phase and amplitude propagation within the nonlinear material by assuming that the sample is thin compared to any changes in the laser beam irradiance distribution due to linear and nonlinear propagation effects. That is, the sample is thin compared to the depth of focus of the beam (i.e. the diffraction length), and compared to distances in which a nonlinearly induced phase distortion can propagate to give amplitude distortion.[16] By choosing the sample thickness and focusing geometry correctly this approximation can be satisfied. If this assumption is not valid the full wave equation must be solved numerically including both spatial and temporal beam characteristics. This often requires a supercomputer. Throughout this paper, we assume the thin sample approximation to be valid. Experimentally the requirement is that the sample thickness  $L$  is less than the diffraction length,  $Z_0 = \pi w_0^2/\lambda$  where  $w_0$  is the half-width at the  $e^{-2}$  of maximum (HW1/e<sup>2</sup>M) of the irradiance distribution and  $\lambda$  is the wavelength in air. In addition, irradiances must be used that give integrated phase shifts less than approximately  $2\pi$ . This situation is also known as "external self-action".[16, 17]

Nonlinear absorption and refraction always coexist (although with different spectral properties) as they result from the same physical mechanisms. They are connected via dispersion relations similar to the usual Kramers-Kronig relations that connect linear absorption to the linear index (or, equivalently, relate the real and imaginary parts of the linear susceptibility).[18-21] The physical processes that give rise to NLA and the accompanying NLR include "ultrafast" bound electronic processes and "excited state" processes, where the response times are dictated by the characteristic formation and decay times of the optically induced excited states. Ultrafast processes include multiphoton absorption [12,19], stimulated Raman scattering [22] and AC-Stark effects [19,20]. Excited-state nonlinearities can be caused by a variety of physical processes including absorption saturation [22], excited-state absorption in atoms and molecules [23] or free-carrier absorption in solids [24,25], photochemical changes [26], as well as defect and color center formation [27]. The above processes can lead to increased transmittance with increasing irradiance (eg. saturation, Stark effect) or decreased transmittance (eg. multiphoton absorption, excited-state absorption). The key to distinguishing these processes is to pay particular attention to the temporal response. One way of achieving this is the use of pulsewidths much shorter than the decay times of the excited states. As we shall show, in this regime, the excited-state nonlinearities are fluence (ie. energy per unit area) dependent, while the ultrafast effects remain irradiance dependent.

It is important to note early in this paper the importance of accurately measuring the laser mode and pulse parameters. For example, two-photon absorption (2PA) is irradiance dependent. Thus, given the pulse energy, we need to know both the beam area (i.e. spatial beam profile) and the temporal pulse width (i.e. temporal shape) in order to determine the irradiance. Any errors in the measurement of irradiance translate to errors in the determination of the 2PA coefficient,  $\beta$ . Similar comments apply to other nonlinearities. Figure 1 shows a plot of  $\beta$ (cm/GW), on a semilogarithmic scale, as a function of year published in the literature for GaAs. It has been established that these large differences are not due to differences in the materials, but are due to experimental problems and interpretation errors. Clearly, there are a great number of pitfalls for experimenters in NLO.

## II.1 Nonlinear absorption:

We will primarily limit our discussion to the increasing loss from two-photon absorption (2PA) and photogenerated excited-state absorption (ESA). The losses from 2PA occur in solids when the photon energy,  $\hbar\omega$ , is larger than one-half the band-gap energy,  $E_g$ . The equation describing 2PA (a third-order response) of a beam of irradiance  $I$  as a function of depth  $z$  in a material is;

$$\frac{dI}{dz} = -(\alpha_0 + \beta I)I, \quad (1)$$

where  $\beta$  is the 2PA coefficient, and the equation includes residual linear absorption of coefficient  $\alpha_0$ . This linear absorption in solids for  $\hbar\omega < E_g$  can come from defects, impurities or band tailing and can often be ignored in good quality materials.

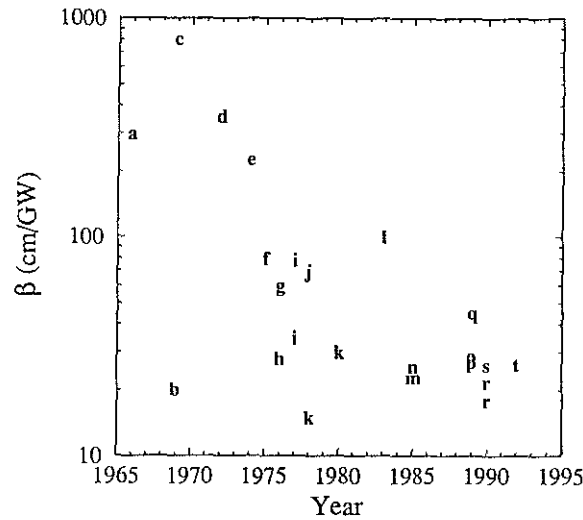


Figure 1. The two-photon absorption coefficient  $\beta$  as a function of year published for GaAs: a [41]; b [42]; c [43]; d [44]; e [45]; f [46]; g [47]; h [48]; i [49]; j [50]; k [51]; l [52]; m [12]; n [53]; o [54]; p [55]; q [56]; r [57]; s [58]; t [25].

Once absorption has taken place, electrons are excited across the energy gap and are available to subsequently absorb linearly. In semiconductors this linear absorption process is known as free-carrier absorption (FCA) and also includes intraband absorption of holes between light and heavy hole bands. In atoms or molecules this process is referred to as ESA. For pulses longer than a few picoseconds (determined by electron-phonon scattering rates) how the carriers were originally excited is irrelevant to the subsequent FCA. However, the equations governing the transmitted irradiance, and the order of the nonlinear response, are intimately tied to the carrier generation process. If linear absorption ( $\alpha_0$ ) creates the carriers (as, for example, in a thin indirect-gap material [24], doped semiconductor, or organic [23]) the equation governing  $I$  (ignoring 2PA) becomes,

$$\frac{dI}{dz} = -(\alpha_0 + \sigma N)I, \quad (2)$$

where  $\sigma$  is the FCA cross section, and  $N$  denotes the density of excited carriers produced by linear absorption. The rate of carrier production is given by

$$\frac{dN}{dt} = \frac{\alpha_0 I}{\hbar\omega}. \quad (3)$$

Here  $\hbar\omega$  is the incident photon energy used to produce an electron-hole pair. We have ignored all decay and diffusion processes that can reduce the carrier density in writing Eq. 3. In general these processes must be included which can greatly complicate the determination of nonlinear parameters, however, if pulses are short compared to the recombination and diffusion times (eg. picosecond pulses), this assumption is valid. An analogous pair of equations is valid for excited-state absorption in atomic or molecular systems where  $N$  is then the density of excited states. By integrating Eq. 3 up

to some time  $t'$  in the pulse, substituting for  $N$  in Eq. 2 and then integrating over all times  $t'$  (i.e.  $-\infty$  to  $\infty$ ) we find the fluence  $F$  varies with  $z$  as

$$\frac{dF}{dz} = - \left[ \alpha_0 + \frac{\alpha_0 \sigma}{2\hbar\omega} F \right] F. \quad (4)$$

Notice that this equation is exactly analogous to Eq. 1 describing 2PA loss with the fluence replacing the irradiance and  $\alpha_0 \sigma / 2\hbar\omega$  replacing  $\beta$ . Therefore, since in most experiments the pulse energy is detected, FCA initiated by linear absorption and 2PA, will give nearly identical results for loss as a function of input energy (microscopically ESA can be considered as the limit of 2PA with a resonant intermediate state). The difference between Eqs. 1 and 4 when determining the transmitted energy is in the temporal integral over the pulse for 2PA. For FCA, this integral has already been performed. In other words, in order to determine which of these nonlinearities is present, the temporal dependence must be measured in some way.

If the carriers are produced via a 2PA process ( $\beta$  in Eq. 1) rather than by linear absorption ( $\alpha_0$  in Eq. 1), the resulting equations are considerably different, and cannot be solved analytically. Including 2PA, Eq. 2 becomes,

$$\frac{dI}{dz} = -(\alpha_0 + \beta I + \sigma N) I, \quad (5)$$

which must now be combined with the 2PA carrier generation rate,

$$\frac{dN}{dt} = \frac{\beta I^2}{2\hbar\omega}. \quad (6)$$

The factor of 2 indicates that the energy of two photons is needed to create the carrier pairs. Again we make the simplifying assumption that carriers do not diffuse or decay during the pulse. In semiconductors, this assumption is normally valid with picosecond pulses. In Eq. 5,  $\alpha_0$  is again included only as a residual linear absorption from defects or impurities, and it is assumed that free carriers are not produced in the process.

It is interesting to look at the order of the nonlinear response for the three cases given above. The first two, 2PA and linearly generated FCA, both appear as third-order responses. However, in one case, 2PA, the nonlinearity is proportional to  $\text{Im}\{\chi^{(3)}\}$ , while for the linear absorption generated FCA the nonlinearity is due to the cascaded process  $\text{Im}\{\chi^{(1)}\}; \text{Im}\{\chi^{(1)}\}$  (i.e. two linear absorption processes), where the first  $\chi^{(1)}$  is associated with the ground state absorption and the second with FCA. Here  $\chi^{(j)}$  refers to the  $j$ th order electric susceptibility. Without knowledge of the temporal dependence of the process, FCA and 2PA are indistinguishable.

For the third case, 2PA generated FCA, the nonlinear response appears fifth order, a cascaded  $\text{Im}\{\chi^{(3)}\}; \text{Im}\{\chi^{(1)}\}$  (i.e. 2PA followed by FCA). However, the overall nonlinear transmission as given by Eq. 5 has both the third-order response of 2PA (second term) and the fifth-order cascaded

response (third term). This can give quite complicated transmission curves as a function of input energy or irradiance. We find similar ambiguities in the interpretation of nonlinear refraction experiments as seen in section II.2 (also see *Results for ZnSe* in section III.2). If pulses having the same peak irradiance but different temporal widths are incident on a material obeying Eqs. 5 and 6, the longer pulses, having more energy, will create more carriers. Thus, the longer pulse will induce more FCA, assuming slow carrier decay times, and suffer more loss. This is a useful method to determine if such processes are present.

The FCA resulting from 2PA generated carriers can be shown [12,28] to be small compared to the direct 2PA process for irradiances below a critical irradiance,  $I_{cr} \simeq 2\sqrt{2}\hbar\omega/\sigma\tau$ , where  $\tau$  is the laser pulsewidth. This is one of several reasons why short pulses are valuable for measuring  $\beta$  without the influence of other nonlinear phenomena. In addition the NLR from these carriers is also reduced for shorter pulses.

The solution to Eq. 1 for 2PA at the exit surface of the sample is

$$I(L, r, t) = \frac{I(0, r, t)e^{-\alpha_0 L}}{1 + q(r, t)} \quad (7)$$

where  $q(r, t) = \beta I(0, r, t)L_{\text{eff}}$ , and  $L_{\text{eff}} = (1 - e^{-\alpha_0 L})/\alpha_0$ . Here, we have explicitly shown the possible time ( $t$ ) and transverse spatial ( $r$ ) dependences of the irradiance. Assuming continuous, spatially homogeneous beams, Eq. 7 can be written in terms of the transmittance, here given by the ratio of irradiances,  $T = I(L)/I(0)$ , as

$$\frac{1}{T} = e^{\alpha_0 L} (1 + \beta I(0)L_{\text{eff}}), \quad (8)$$

where Fresnel reflections are ignored. This simple expression has led to the historical method of measuring the transmittance as a function of input irradiance  $I(0)$ , and plotting  $T^{-1}$  versus  $I(0)$ . [12,28] The result is a straight line, the slope of which determines  $\beta$ , and the intercept gives  $\alpha_0$ . There is only a small deviation from this straight line dependence when integrals over the spatial and temporal profiles are included (see Fig. 2).

Analogous to the case of 2PA, the solution of Eq. 4 for linear absorption generated FCA is

$$F(L, r) = \frac{F(0, r)e^{-\alpha_0 L}}{1 + p(r)} \quad (9)$$

where  $p(r) = (\alpha_0 \sigma / 2\hbar\omega) F(0, r)L_{\text{eff}}$ . Equation 9 for FCA gives a result similar to Eq. 8 for 2PA but is a function of the input fluence,  $F(0)$ . That is, assuming a spatially uniform beam,

$$\frac{1}{T} = e^{\alpha_0 L} \left[ 1 + \frac{\alpha_0 \sigma}{2\hbar\omega} F(0)L_{\text{eff}} \right], \quad (10)$$

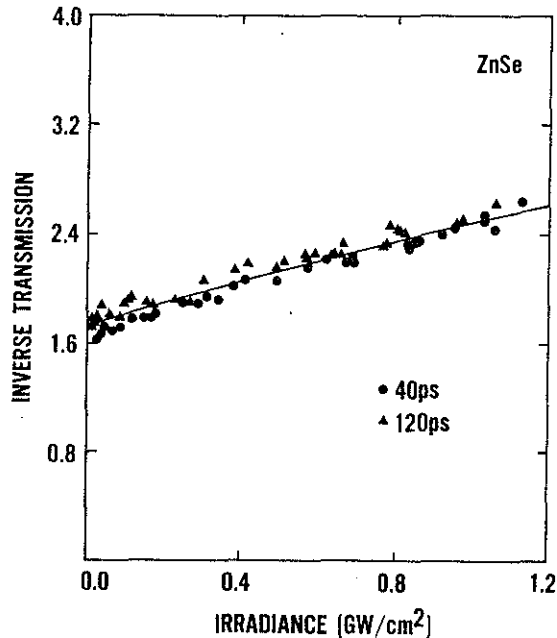


Figure 2. Inverse transmittance for ZnSe as a function of the external incident irradiance using input pulsewidths of 40 psec and 120 psec (FWHM).

where now  $T$  is defined as the ratio of output to input fluence. Again, including an integral over the spatial distribution only gives a small deviation from the straight line prediction of Eq. 10 whose slope, in conjunction with the intercept, now determines  $\sigma$ . In experiments to determine  $T$ , it is usually the pulse transmitted energy,  $E$ , that is monitored, meaning that the spatial and temporal integrals for 2PA, or the spatial integral for linearly generated FCA, must be performed. Thus, for a single experiment of  $T = E(L)/E(0)$  versus the input energy, these very different nonlinear processes are indistinguishable. Only if the temporal dependence of the transmittance were directly monitored could these two processes be distinguished.

This is a very important distinction between a direct  $\chi^{(3)}$  response and a sequential, cascaded  $\chi^{(1)}:\chi^{(1)}$  response. In general, many processes can have a third-order response but may not be strictly described by a  $\chi^{(3)}$  susceptibility. Thermal nonlinearities, excited-state nonlinearities, electrostrictive nonlinearities, etc. are examples, and this statement is valid for absorptive ( $\text{Im } \chi^{(3)}$ ) and refractive ( $\text{Re } \chi^{(3)}$ ) responses. For example, a thermal nonlinearity is normally described by a  $\chi^{(1)}:\chi^{(1)}$  response. The sample first linearly absorbs the light which changes its temperature ( $\text{Im } \chi^{(1)}$ ). This temperature change, in turn, changes the linear absorption ( $\text{Im } \chi^{(1)}$ ) or changes the linear refractive index ( $\text{Re } \chi^{(1)}$ ). This latter effect is referred to as thermal lensing or thermal blooming as it is often a defocusing effect. The turn-on time for thermal effects depends upon the mechanism for the induced changes in  $\chi^{(1)}$ . For example, lattice heating induces a change in bandgap that, in time,

alters the spectrum of  $\text{Re}\{\chi^{(1)}\}$  and  $\text{Im}\{\chi^{(1)}\}$ . The turn-on time for this is dictated by the rate at which heat is given to the lattice, a combination of electron phonon inelastic scattering rates and nonradiative recombination rates. If the index is changed by thermal expansion of the medium, which is usually the dominant process in liquids, the turn-on time is given by the transit time of an acoustic wave across the beam. In both cases the decay time is dictated by thermal diffusion. The determination of the underlying physics describing the nonlinear response is the major point to be made in this paper.

Section III demonstrates how the dominant loss mechanism is experimentally determined by observing the pulsewidth dependence of the nonlinear absorption. Such experiments are also useful for determining NLR mechanisms as discussed below.

## II.2 Nonlinear Refraction:

As discussed in section II, NLR always accompanies NLA and results from the same physical mechanisms. Just as 2PA is a physical process that can be described in terms of  $\text{Im}\{\chi^{(3)}\}$ , there is a corresponding  $\text{Re}\{\chi^{(3)}\}$  that describes ultrafast nonlinear refraction. The same is true for cascaded processes.

The induced phase distortion imposed on a laser beam by NLR is related to the index change,  $\Delta n$ , by

$$\frac{d\phi}{dz} = \frac{\Delta n 2\pi}{\lambda}. \quad (11)$$

The refractive index can be changed from the same large variety of mechanisms that can change the absorption. We, for example, discussed thermal effects in the previous section. Here we discuss the bound-electronic nonlinear refraction characterized by  $n_2$  and excited-state or free-carrier refraction (ESR or FCR). We restrict the use of  $n_2$  here to only the ultrafast electronic response. FCR has its analogue in atomic and molecular systems where the NLR comes from the redistribution of population among levels. For example, in a two-level system, the absorption saturates which by causality [20] changes the refractive index. In solids this redistribution generates free carriers which block further transitions (Drude band blocking) and the refractive index is changed (i.e. FCR).[25,29]

Defining  $\sigma_r 2\pi/\lambda$  as the change in index of refraction per unit of photoexcitation density,  $N$ ,  $\Delta n$  in Eq. 11 is written as;

$$\Delta n = n_2 I + \frac{\lambda}{2\pi} \sigma_r N. \quad (12)$$

Here  $\sigma_r$  is the FCR cross section (often the  $2\pi/\lambda$  is dropped in the definition of the index change), and  $n_2$  is in units of  $\text{m}^2/\text{W}$ . The nonlinear index,  $n_2$ , due to bound electrons can also be expressed in Gaussian units as  $\Delta n = n_2 |E|^2/2$ , where  $n_2$  is in units of  $(\text{cm/statvolt})^2$ , or esu.  $n_2(\text{MKS})$  is related to  $n_2(\text{esu})$  through  $n_2(\text{esu}) = (cn_0/40\pi) n_2(\text{MKS})$ , with  $c$  the speed of light in  $\text{m}/\text{sec}$ .

For the case where free carriers are generated from single photon absorption processes (see Eq. 3),

$$\Delta n(t) = n_2 I(t) + \frac{\alpha_0 \sigma_r}{\hbar \omega} \int_{-\infty}^t I(t') dt' . \quad (13)$$

The bound electronic response follows the temporal dependence of the pulse input while the FCR builds up in time through the pulse. For the case where the carriers are created solely by 2PA (see Eq. 6) Eq. 12 becomes,

$$\Delta n(t) = n_2 I(t) + \frac{\beta \sigma_r}{2 \hbar \omega} \int_{-\infty}^t I^2(t') dt' . \quad (14)$$

Usually, especially when using picosecond or shorter pulses, the phase distortion is not time resolved and only the temporally averaged value is measured. Assuming the nonlinear refraction accumulates throughout the pulse without decay, it can be shown that the temporally averaged index change is simply one half  $\Delta n_{FC}(t=\infty)$  or it equals  $\Delta n_{FC}(t=0)$  for a symmetric pulse in time.[11] Here,  $\Delta n_{FC}$  refers to the second term in Eq. 13 or 14. The contribution from the bound electronic  $n_2$  (first term in Eq. 14) gives an index change  $\Delta n_{n_2}$ , averaged over a Gaussian temporal pulse, of  $1/\sqrt{2}$  times the peak value. Thus, the temporally averaged index change is,

$$\langle \Delta n \rangle = \frac{1}{\sqrt{2}} n_2 I(t=0) + \frac{1}{2} \Delta n_{FC}(t=0) . \quad (15)$$

Integrating Eq. 11 over the sample length to obtain the total phase distortion  $\Delta \phi(r, t)$ , we define  $\langle \Delta \phi \rangle$  as the temporally averaged phase distortion as determined from Eq. 15. We then define  $\Delta \Phi$  as  $\Delta \phi$  evaluated at the beam center ( $r=0$ ), with similar definitions for the temporally averaged quantities, eg.  $\langle \Delta \Phi \rangle$  is the on-axis temporally averaged phase distortion.

$\Delta \phi$  can also be a periodic function of the spatial coordinates  $x$  (or  $y$ ) due to the interference of two or more coherent beams as in, for example, DFWM (discussed in section III.2). Beam propagation and diffraction are discussed in the next section along with experimental techniques.

### III. Experimental Techniques

In a single article it would be impractical to satisfactorily describe the many experimental techniques to measure NLA and NLR, so we choose to give just three examples. We describe direct transmission measurements, Z-scan and temporally-resolved DFWM. We discuss the complementary information that these methods give. This choice only reflects the fact that the authors are most familiar with these techniques. In addition this article does not discuss methods that measure nonlinearities in fibers or waveguides; however, these three methods can measure nonlinearities of the constituent materials in bulk or thin film form. In general it is best to use as many complementary experimental techniques as possible to determine the nonlinear optical response of a given material.

## III.1 Nonlinear Transmittance

Perhaps the simplest method to measure NLA is to monitor the energy transmitted by a sample as a function of the input energy. We choose energy since normally the irradiance needed to give significant absorption is  $\approx 10^7$  W/cm<sup>2</sup> or higher and short pulses (difficult to time resolve) are extremely valuable to reduce competing nonlinearities.

Figure 2 shows experimental results for the inverse transmittance of a 2.7 mm thick chemical-vapor deposition grown (polycrystalline) sample of ZnSe (linear index  $n=2.7$ ) plotted as a function of the external input irradiance using two different picosecond pulsewidths at 532 nm. ZnSe has an energy gap of  $E_g \approx 2.6$  eV and, therefore, displays 2PA at 532 nm.[25] Since the horizontal axis is irradiance and not energy the fact that the different pulsewidths give the same change in transmittance shows that Eq. 1 for 2PA is consistent with the measurement.

Many of the discrepancies between values for  $\beta$  shown in Fig. 1 come from the use of nanosecond rather than picosecond pulses. Longer pulses can make competing nonlinear absorption processes such as 2PA induced FCA dominant (see Eq. 5), leading to larger losses than from 2PA alone. Not accounting for such effects results in overestimation of  $\beta$ , sometimes by orders of magnitude. An additional problem in transmission experiments is the seemingly simple task of collecting all the transmitted beam. Due to the NLR that accompanies 2PA the beam can rapidly spread after

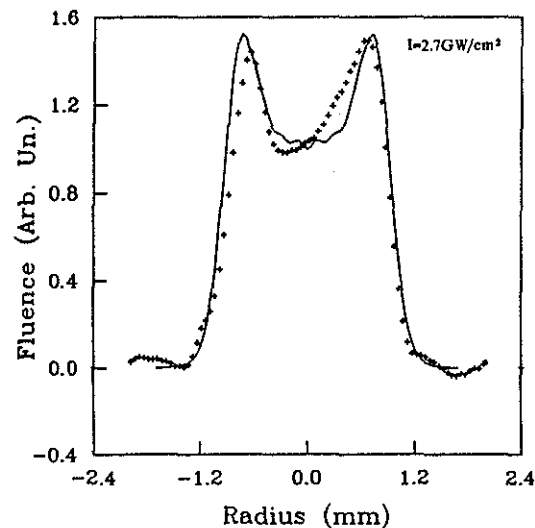


Figure 3. Spatial beam profile (+s) through the center of an originally Gaussian profile beam after transmission through a 2.7 mm thick CVD grown ZnSe sample and  $\approx 55$  cm free space propagation to a vidicon detector. The input irradiance is 2.7 GW/cm<sup>2</sup>. The solid line is a theoretical calculation using values for the nonlinear coefficients as determined by Z-scan measurements as discussed in the text.

traversing the sample. Figure 3 shows a transverse scan through the center of an initially Gaussian spatial profile beam (30 ps FWHM pulse at 532 nm,  $Z_0=178$  cm) after transmission through the ZnSe and then propagating 55 cm to the vidicon (near field). The beam breakup into two peaks is characteristic of a self-defocusing (negative induced lens) nonlinearity in the near field. This effect can become very strong at high irradiance and is enhanced for longer pulsewidths (having more energy) by free-carrier refraction. While a detector placed after the sample collects all the beam at low inputs, the detector can miss some of the light at high inputs. Again these effects result in an overestimation of  $\beta$  (see Fig. 1).

While FCA can be negligible for picosecond pulses (see discussion in section II.1), the refraction arising from these free carriers, FCR is not.[12] As shown in Fig. 3, ZnSe displays strong self defocusing even for picosecond pulses. As discussed in section III.2, this defocusing is a combination of bound-electronic and free-carrier refraction as described by Eq. 14 (and 15). The solid line in Fig. 3 shows results of a computer calculation using parameters obtained from Z-scans (see section III.2). The field at the exit surface of the sample is determined by  $E \propto \sqrt{I} e^{i\phi}$ , and as described in Ref. [25], this field is propagated to the vidicon detector to give the results of Fig. 3. We discuss this further in the next section.

### III.2 Z-SCAN

Z-scan measures both the nonlinear loss and phase distortion imposed on a Gaussian beam.[10,11] For measuring NLR this technique exploits the spatial narrowing and broadening of Gaussian beams in the far field which are due to self-focusing or self-defocusing caused by the nonlinear interaction of the beam with the material. A schematic of the experimental setup is given in Fig. 4. A Gaussian beam is focused onto the sample and then collected through an aperture in the far field by the transmission detector ( $D_2$ ). Keeping the input energy constant, the sample is translated along the beam propagation direction through the focal plane, and the transmittance ( $D_2/D_1$ ) is measured as a function of this sample position  $Z$  with respect to the focal plane ( $Z$  should not be confused with  $z$ , the depth within the sample). In the case of a material with a negative nonlinear refractive index, the self-defocusing will cause beam narrowing in the far field when the sample is before focus (negative  $Z$ ) and beam broadening when the sample is after focus (positive  $Z$ ). An increase in transmittance followed by a decrease in transmittance (peak-valley) for increasing  $Z$  denotes negative nonlinear refraction, while a valley-peak configuration implies positive nonlinearity. In Ref. [11] we give a detailed description and analysis of the Z-scan technique. Within the thin sample approximation [16,17], it is found that the change in the index of refraction ( $\Delta n$ ) is given by a linear relation between the on-axis temporally averaged phase distortion at focus ( $\langle \Delta \Phi_0 \rangle$ ) (where the subscript on  $\Phi$  refers to the sample positioned at the beam waist, i.e. at focus) and the difference between the maximum and minimum values of the normalized aperture transmittance,  $\Delta T_{pv}$ . This relation for an aperture size that gives 40% linear transmittance is given by:[11]

$$\langle \Delta \Phi_0 \rangle \simeq 2.8 \Delta T_{pv} . \quad (16)$$

Examining Fig. 4 for a purely refractive case, if the aperture is removed i.e. if all the transmitted

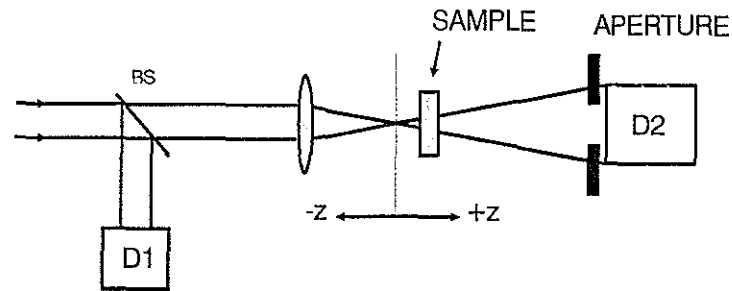


Figure 4. The Z-scan experimental setup.  $D_2/D_1$  is measured as a function of the sample position  $z$ .

light from the sample is collected by  $D_2$ , there will be no change in the transmittance at different sample positions. However, if the sample exhibits nonlinear absorption, the measurement will detect the nonlinear loss which is maximized at  $Z=0$ . This type of measurement, to which we refer as an "open aperture" Z-scan, yields the nonlinear absorption parameters of the material. When the aperture is in place, the measurement (closed aperture Z-scan) is sensitive to both nonlinear absorption and nonlinear refraction. Dividing the closed aperture data by the open aperture data yields a Z-scan curve due only to nonlinear refraction which can be determined using Eq. 16 as long as the nonlinear absorption is not too strong. Figure 5 shows an example of this procedure for ZnSe where picosecond 532 nm pulses were used. Figure 5(a) and 5(b) show open aperture and closed aperture results respectively, while Fig. 5(c) shows the results of the division of 5(b) by 5(c). The solid lines are fits as discussed later under "results for ZnSe". The limitations of this simple approach and when a more exact analysis is needed are described in detail in Ref. [11].

The open aperture Z-scan, or measuring the change in transmittance as a function of irradiance,  $I$ , is a relatively straightforward experiment as long as care is taken to collect all the light transmitted by the sample and the detectors used have uniform response (i.e. if the light is spread over a larger or smaller surface area the detector response is unchanged).

As a final comment, we note that the Z-scan curve can serve as a calibration on the input fluence. The distance in  $Z$  between the peak and valley for a Gaussian beam and a third-order nonlinearity is given by  $\Delta Z_{pv} \approx 1.7 Z_0$ . Thus, a Z-scan gives the the beam size. This is a very convenient method to use if the nonlinear response is understood. On the other hand, once the system is calibrated, the Z-scan shape also contains information concerning the order of the nonlinearity. For example, a fifth-order response has a narrower Z-scan curve with  $\Delta Z_{pv} \approx 1.2 Z_0$  [11]

The following experiments on the semiconductor ZnSe illustrate the complexity of the nonlinear interactions even for picosecond pulses, and the difficulties in unraveling the different nonlinear processes.

#### *Results for ZnSe*

With 27 picosecond (FWHM) pulses at 532 nm from a frequency doubled Nd:YAG laser we

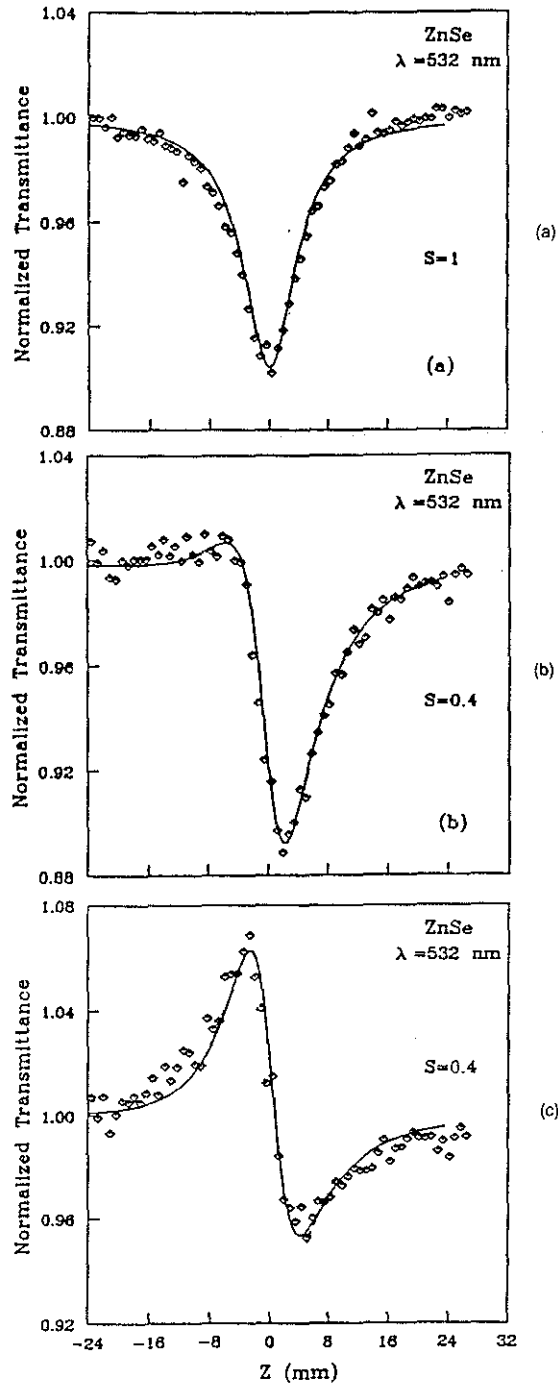


Figure 5. Normalized Z-scan transmittance of ZnSe measured using picosecond pulses at  $\lambda = 532$  nm with  $I_0 = 0.21$  GW/cm<sup>2</sup>. (a) Open aperture data and fit (solid line) (b) 40% aperture data and fit (solid line) and (c) The result of the division of the Z-scans of (a) and (b).

performed Z-scans at different input energies on the 2.7 mm thick polycrystalline ZnSe sample. The beam was focused to give  $w_0 \approx 25 \mu\text{m}$ . First, an open aperture Z-scan was performed. In Fig. 5(a) we plot the experimental data. In addition we show a numerically calculated Z-scan using  $\beta = 5.8 \text{ cm/GW}$  and  $\alpha_0 = 0.3 \text{ cm}^{-1}$  in Eq. 7 including spatial and temporal integrals. The Z (as opposed to the depth  $z$ ) dependence is introduced in the irradiance  $I$  in Eq. 7 by the standard Gaussian beam propagation equation,

$$I(Z) = \frac{I(0)}{1+(Z/Z_0)^2} \quad (17)$$

giving a Lorentzian shaped curve for loss versus Z.

With a 40% linearly transmitting aperture a closed aperture Z-scan was performed at the same irradiance (Fig. 5b). In this case the measurement is sensitive to both NLR and NLA. Experiments on ZnSe were conducted at peak irradiance levels from  $I_0 = 0.21 \text{ GW/cm}^2$  to  $2.4 \text{ GW/cm}^2$ . The experimental irradiances are within the sample (i.e. Fresnel reflections taken into account).

In all, ten Z-scans were performed (5 "open" aperture and 5 "closed"). Closed aperture Z-scans at a peak input irradiance of  $0.57 \text{ GW/cm}^2$  and  $2.4 \text{ GW/cm}^2$  are shown in Fig. 6a and 6b respectively. Open aperture Z-scans show a third-order response and a strictly irradiance dependent loss as confirmed by using different pulsewidths (see Fig. 2). This confirms that 2PA is the dominant nonlinear loss mechanism and a value of  $\beta \approx 5.8 \text{ cm/GW}$  is obtained as shown by the fit to the data of Fig. 5a.

Using the 40% aperture Z-scan and dividing out the nonlinear absorption, we calculate  $\Delta n$  from the phase shift data (i.e. using Eqs. 11 and 16).[25] Plotted in Fig. 7 is  $\Delta n/I_0$  versus the peak input irradiance  $I_0$ . If this graph showed a horizontal straight line we could interpret this as a third-order response, and since we are using picosecond pulses in a spectral range where there is little linear absorption, we could conclude that it is most likely due to the third-order anharmonic motion of the bound electrons (i.e.  $n_2$ ).[11,25] Performing Z-scans at different pulsewidths, with pulses shorter than carrier decay rates, could confirm this conclusion by showing a strict irradiance dependence rather than a fluence dependence as would be indicative of linearly generated FCR. The negative slope of the line in Fig. 7 indicates a higher order self-defocusing. Since the graph shows a linear dependence we conclude a fifth order response consistent with 2PA generated FCR. The intercept of this line gives a fitted value of  $n_2 \approx -6.4 \times 10^{-14} \text{ cm}^2/\text{W}$  ( $-4.1 \times 10^{-11} \text{ esu}$ ) and the slope gives  $\sigma_r 2\pi/\lambda \approx -1.1 \times 10^{-21} \text{ cm}^3$ . The details of how this simple method is used to estimate these numbers is given in Ref. [25].

With  $\beta \approx 5.8 \text{ cm/GW}$  we also performed a complete numerical fit to the Z-scans. Using an iterative approach to best fit all the data, we found a better fit with  $n_2 \approx -6.2 \times 10^{-14} \text{ cm}^2/\text{W}$  ( $-4.0 \times 10^{-11} \text{ esu}$ ), and  $\sigma_r \lambda/2\pi \approx -0.8 \times 10^{-21} \text{ cm}^3$  ( $\sigma_r \approx -9 \times 10^{-17} \text{ cm}^2$ ). The solid lines shown in Fig. 5 are the fits to the data. These numbers were also used to give the theoretical curve of the beam profile shown in Fig. 3.

We also measured  $n_2$  in ZnSe at  $1.06 \mu\text{m}$  where 2PA is not present. Using 40 ps pulses (FWHM) from a Nd:YAG laser focused to  $w_0 \approx 40 \mu\text{m}$ , we obtained  $n_2 = +2.9 \times 10^{-14} \text{ cm}^2/\text{W}$  ( $+1.7 \times 10^{-11} \text{ esu}$ ). In Fig. 8 we plot closed aperture Z-scans obtained in ZnSe at  $1.06 \mu\text{m}$  and at  $0.53 \mu\text{m}$  showing the change in sign of  $n_2$ . In this figure, the nonlinear absorption has been divided out of the  $0.53 \mu\text{m}$  data. This observed dispersion in  $n_2$  and change in sign is consistent with the recent theory of Refs. [19-21] and shows the necessity of measuring the nonlinearity at more than a single wavelength.

In addition to separately measuring NLA and NLR, Z-scan can be used to determine the anisotropy of these responses (eg. the different responses to linear and circular polarized light). This is

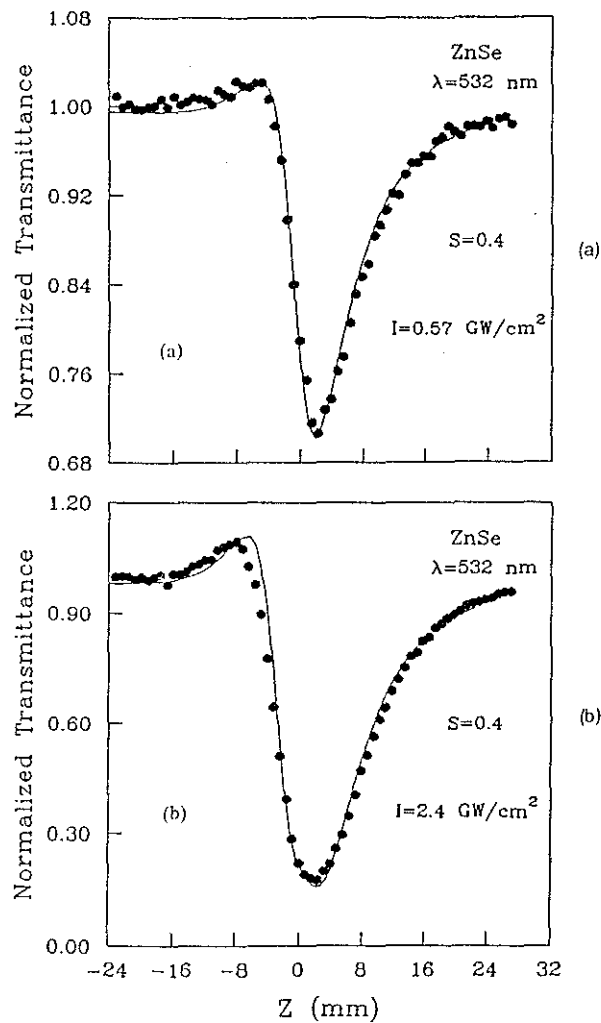


Figure 6. Closed aperture Z-scan data ( $S=0.4$ ) and theoretical fit (solid lines) of the ZnSe sample taken at irradiance levels of  $I_0=0.57 \text{ GW/cm}^2$  (a) and  $I_0=2.4 \text{ GW/cm}^2$  (b) where free-carrier refraction is large.

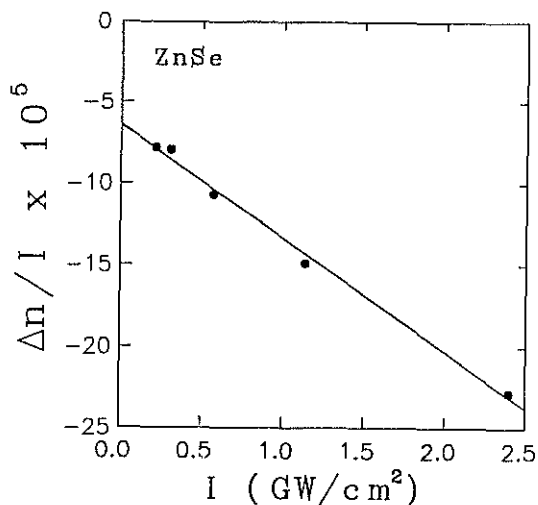


Figure 7.  $\Delta n/I_0$  directly derived from  $\Delta T_{pv}$  plotted as a function of  $I_0$  for ZnSe.

particularly important for single crystal materials. We recently applied these methods to single crystals of GaAs, BaF<sub>2</sub> and KTP to determine various  $\chi^{(3)}$  tensor elements.[30]

One of the difficulties in the interpretation of the Z-scan data is the absence of temporal information. Recently we introduced a temporally resolved, 2-color Z-scan that can separately give the temporal evolution of the NLA and NLR.[31] Next, however, we describe the use of picosecond DFWM to time resolve the nonlinear response.

### III.2 Degenerate Four-Wave Mixing

In the experiments described here, the standard "backward" DFWM geometry is used.[3,32,33] A schematic of the experimental geometry using single 43 ps (FWHM) 1.064  $\mu\text{m}$  pulses, or 30 ps (FWHM) 0.532  $\mu\text{m}$  pulses is shown in Fig. 9. The single pulse input is divided into three pulses which, after passing through variable time delays, are incident on the sample. The three pulses can be independently adjusted in amplitude and polarization using half-wave plate and polarizer combinations. Two strong beams, forward ( $E_f$ ) and backward ( $E_b$ ) pumps, of approximately equal irradiance are incident on the sample from counterpropagating directions. A weaker beam, the probe ( $E_p$ ), is incident on the sample at an angle  $\theta$  with respect to  $E_f$ .

The physical operation of this technique involves scattering of one of the strong pump pulses off the grating produced by the interference of the probe with the other pump through the nonlinear modulation of the refractive index and/or absorption coefficient. The grating is only formed by a *nonlinear* interaction of the light with the material. While this is a somewhat simplified physical interpretation (eg. it doesn't describe two-photon coherence effects [3]), it suffices for most experiments. Thus, assuming all beams are linearly polarized parallel to each other, there are two

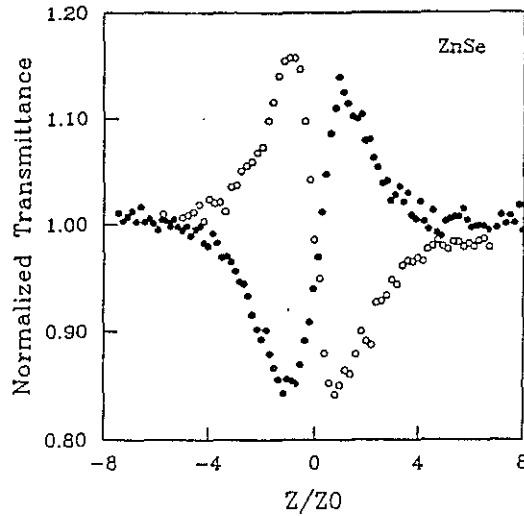


Figure 8. Closed aperture ( $S=0.4$ ) Z-scan experimental data (filled circles) of ZnSe at  $1.06 \mu\text{m}$  and  $532 \text{ nm}$  (open circles) in units of  $Z_0 = \pi w_0^2/\lambda$ . This figure clearly shows the dispersion in  $n_2$  as it changes sign from positive at  $1.06 \mu\text{m}$  to negative at  $532 \text{ nm}$ .

amplitude gratings formed that can diffract a pump beam; one between  $E_t$  and  $E_p$ , and the other between  $E_b$  and  $E_p$ . The grating spacing is determined by the angle  $\theta$  which is usually made to be small (a few degrees). In this case, one of the gratings has a spacing larger than  $\lambda$  ( $\approx \lambda/\theta n$ ) while the other has a spacing of  $\approx \lambda/n$ . Calculating the direction of the beam diffracted off either of these gratings shows that this field,  $E_c$  (the conjugate wave), retraces the path of  $E_p$  (i.e. the sample retroreflects the beam). This retroreflection is the basis for phase conjugation and phase-conjugate

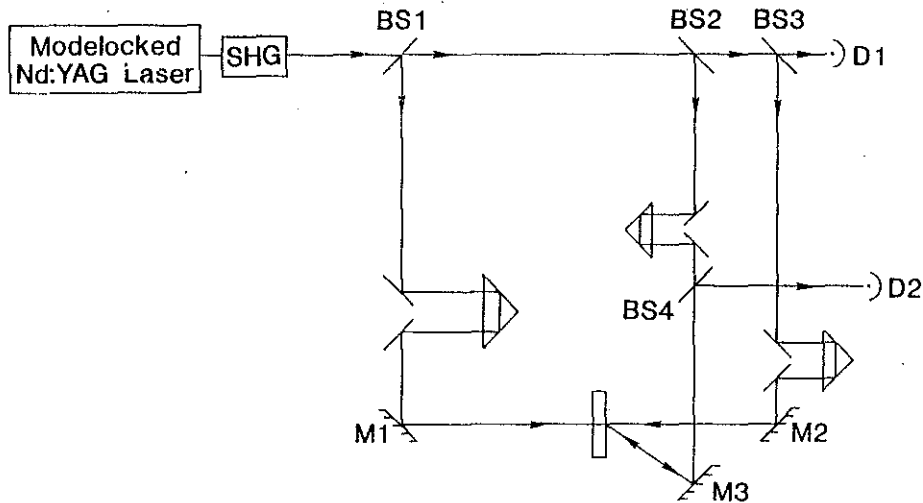


Figure 9. Schematic of experimental DFWM apparatus.  $D_1$  is the input pulse energy monitor, while  $D_2$  monitors the phase-conjugate signal pulse energy.

mirrors.[34] If the beams that write the grating are not polarized parallel, there is a polarization grating formed in the material that can diffract light if the effective nonlinear susceptibility tensor has nonzero off diagonal elements (i.e. polarized light can induce an anisotropy).[34,35] The different DFWM signals obtained using different polarization combinations are useful for determining the various tensor components of the nonlinear electric susceptibility (eg.  $\chi^{(3)}$ ).

Given the above physical interpretation, *any* spatial modulation of the optical properties of the material, index or amplitude grating, will give rise to  $E_c$ . Herein lies the major difficulty with this method in characterizing nonlinear material coefficients. Both NLA and NLR give rise to a similar measured response, thus making it difficult to determine the origin of the nonlinearity. However, by temporally delaying one beam with respect to the others, the lifetimes of the various gratings can be determined which is helpful in determining mechanisms (this is similar to the information obtained by performing pulsewidth dependent studies in transmission or using Z-scan). In what follows we show how DFWM can be used to characterize nonlinearities using ZnSe at an input wavelength of 532 nm as an example.

#### *DFWM in ZnSe*

The DFWM signal in ZnSe is monitored as a function of input energy and pulse delay for different combinations of the polarization of the three input beams. Figure 10 shows a plot of the DFWM signal versus the temporal delay  $\tau_b$  of  $E_b$ , with  $E_b$  polarized perpendicular to both  $E_t$  and  $E_p$  ( $\theta=13^\circ$ ,  $I_b \approx 34$  MW/cm<sup>2</sup> and  $I_t \approx 22$  MW/cm<sup>2</sup>). This polarization combination results in an interference between  $E_t$  and  $E_p$  so that  $E_b$  is diffracted into  $E_c$  off either amplitude or phase gratings induced by this interference. In addition there can be polarization gratings which can also diffract light into  $E_c$ . In this arrangement (Fig. 10) no signal is observed for  $E_b$  incident prior to the other two beams, the grating rapidly forms reaching a maximum near zero time delay and then decays. Clearly, two very distinct nonlinearities are evident from Figure 10. Near zero delay, a large rapidly decaying signal is seen, while at longer delays, we observe a more slowly decaying signal. To better understand the two nonlinear regimes, irradiance dependence experiments were performed at different delays. Figure 11 shows a log-log plot of the DFWM signal versus the total input irradiance, (all three input beams were varied simultaneously) at two different delay times. The line in Fig. 10 labeled (a) shows the irradiance dependence at zero delay which follows a power dependence of  $I^{3.1 \pm 0.2}$ , indicative of a third-order nonlinearity. This could be explained by either 2PA,  $n_2$ , or linearly generated FCR. FCA was ruled out by the results of Fig. 2 as our irradiance is less than  $I_{cr}$ . However, as seen in Fig. 10, this third-order response, with a peak near  $\tau=0$ , lasts for only a time of the order of the pulsewidth. If FCR were responsible, the grating would last as long as the carriers remained excited and did not diffuse to wash out the grating. For many semiconductors, with carrier lifetimes  $\geq 10^{-9}$  s and grating spacings of the order of micrometers, diffusion dominates the grating decay. By performing experiments for different values of  $\theta$  (i.e. different grating spacings), the fast component of response is unchanged. The decay of this fast component is too fast to attribute to decay of the carrier grating. The line in Fig. 11 labeled (b) shows the dependence at a delay of 240 ps, where  $E_b$  is no longer temporally coincident with the other two beams, giving a power dependence of  $I^{5.0 \pm 0.2}$ . The fifth order dependence of the DFWM signal on the input beams is consistent with 2PA generated

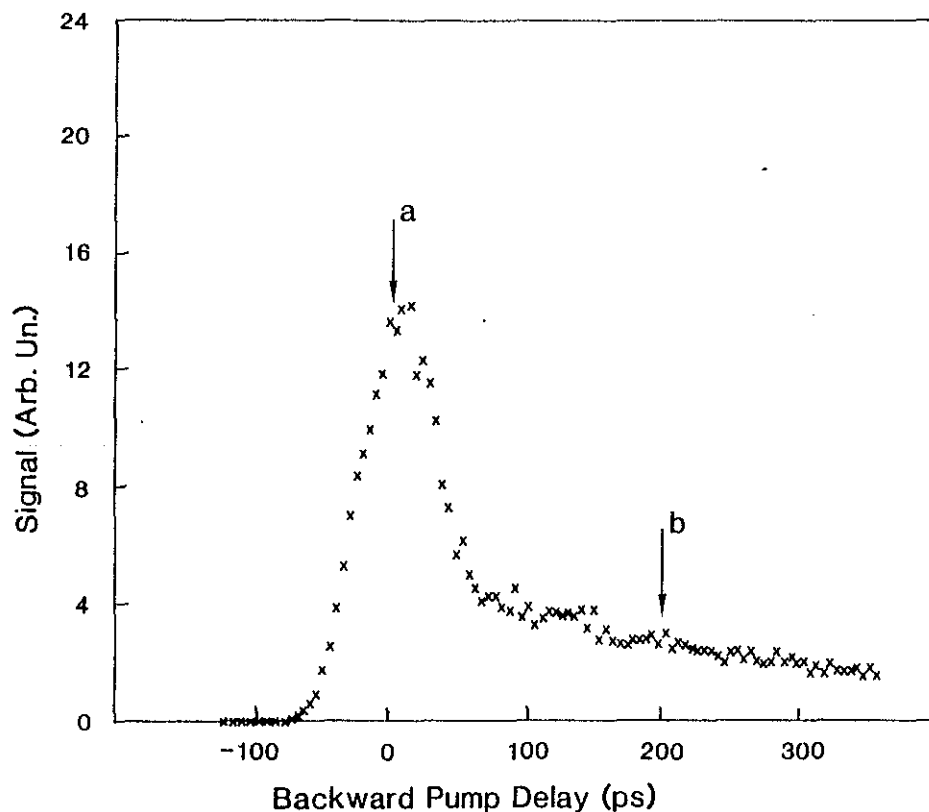


Figure 10. A plot of the phase-conjugate signal versus backward pump delay with the backward pump polarized perpendicular to the other two waves.

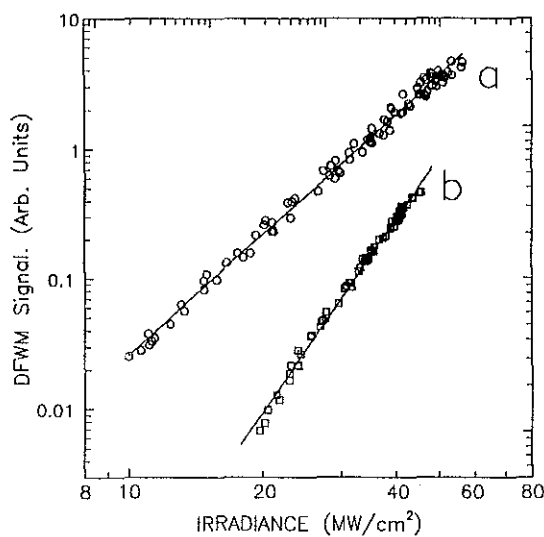


Figure 11. Log-log plots of the phase conjugate signal versus the total input irradiance ( $I_r + I_b + I_p$ ) as all three beams were varied together, for (a) zero delay and (b) 240 ps delay. The solid lines are best fits to the data giving power dependencies of  $I^{3.1 \pm 0.2}$  and  $I^{5.0 \pm 0.2}$ , respectively.

FCR as discussed previously. Studies in other two-photon absorbing semiconductors, such as CdTe at 1.06  $\mu\text{m}$ , reveal the same basic behavior, i.e. a fast third-order signal followed by a slowly decaying fifth-order signal. The results obtained from the DFWM experiments help to confirm the Z-scan results. Thus, the rapidly responding signal near zero delay in Fig. 10 is due to a combination of 2PA and  $n_2$  ( $|\chi^{(3)}|^2 = [\text{Im } \chi^{(3)}]^2 + [\text{Re } \chi^{(3)}]^2$ ), while the slowly decaying signal is due to FCR (the real part of an effective fifth order nonlinearity).[25,35]

#### IV. Frequency Dependence

Having performed picosecond experiments on a number of different materials using transmission and/or Z-scan and/or DFWM we have observed many similarities. If the photon energy is less than one half  $E_g$ , the bound electronic nonlinear refraction dominates the nonlinear response and  $n_2 > 0$  (if very high irradiance is used we have occasionally observed 3-photon absorption when energetically allowed prior to damage). Above one half  $E_g$ , the nonlinear response is complicated by both 2PA and 2PA generated FCR. At very high irradiance the associated FCA can also become significant prior to damage. In addition we find that  $n_2$  becomes negative for photon energies above approximately  $3/4 E_g$ . Figure 8 shows this sign change for ZnSe.

To determine the spectrum of 2PA and the dispersion of  $n_2$ , it would be best to perform the above series of experiments as a function of  $\hbar\omega$ . This is often extremely difficult since the range of frequencies needed can be extremely large (i.e. the transparency range) and tuneable sources with the required irradiance, pulsewidth and beam quality are not typically available. However, using some very simple scaling rules some remarkable relations can be observed. Wherrett [39] has shown that the third-order nonlinear susceptibility  $\chi^{(3)}$  in inorganic solids should scale as

$$\chi^{(3)} \simeq \frac{1}{E_g^4} f(\hbar\omega/E_g), \quad (18)$$

where the complex function  $f$  depends only on the ratio  $\hbar\omega/E_g$  (i.e. upon which states are optically coupled). The nonlinear coefficients  $\beta$  and  $n_2$  are related to  $\chi^{(3)}$  by;

$$\begin{aligned} \beta(\hbar\omega/E_g) \propto \frac{\hbar\omega}{n_0} \text{Im}\{\chi^{(3)}\} &\propto \frac{1}{n_0^2 E_g^3} \frac{\hbar\omega}{E_g} \text{Im}\{f(\hbar\omega/E_g)\} \\ &\propto \frac{1}{n_0^2 E_g^3} F(\hbar\omega/E_g) \end{aligned} \quad (19)$$

and

$$n_2(\hbar\omega/E_g) \propto \text{Re}\{\chi^{(3)}\} \propto \frac{1}{n_0 E_g^4} G(\hbar\omega/E_g) \quad (20)$$

where the defined functions  $F$  and  $G$  are band structure dependent. Thus,  $F$  gives the 2PA spectrum and  $G$  gives the dispersion of  $n_2$ . One method to test the above scaling relations is to scale the

experimental data to obtain the experimental functions;

$$F^e(\hbar\omega/E_g) = \frac{1}{K\sqrt{E_p}} n_0^2 E_g^3 \beta^e \quad (21)$$

and

$$G^e(\hbar\omega/E_g) = \frac{1}{K'\sqrt{E_p}} n_0 E_g^4 n_2^e \quad (22)$$

where  $\beta^e$  and  $n_2^e$  are experimental values of  $\beta$  and  $n_2$ , and  $K$  and  $K'$  are proportionality constants. Here  $E_p$  is the Kane energy as discussed in Ref. [12, 19, 39] and is nearly material independent with a value near 21 eV. Figures 12 and 13 plot these scaled data versus photon  $\hbar\omega/E_g$ , along with the predicted dependence from a two-parabolic band model using a value of  $K=3100$  in units such that  $E_p$  and  $E_g$  are in eV and  $\beta$  is in cm/GW [18-20]. The value of  $K'=0.94 \times 10^8$  is determined from the Kramers-Kronig integral of the nonlinear absorption spectrum using the above value for  $K$ . [19] The data shown in Fig. 12 come primarily from direct transmittance measurements. [12] The data in Fig. 13 for semiconductors come from Z-scan measurements [19] and for dielectrics come from Z-scan [19] and nearly degenerate three-wave mixing [40]. Several materials have now been measured by both techniques and the agreement for  $n_2$  is excellent. As seen in Fig. 12 the experimental 2PA appears nearly step-function like, turning on at approximately  $E_g/2$ . Figure 13 shows a small, positive, nearly dispersionless  $n_2$  for  $\hbar\omega/E_g$  much less than  $E_g$ , reaching a peak near  $E_g/2$ , where 2PA

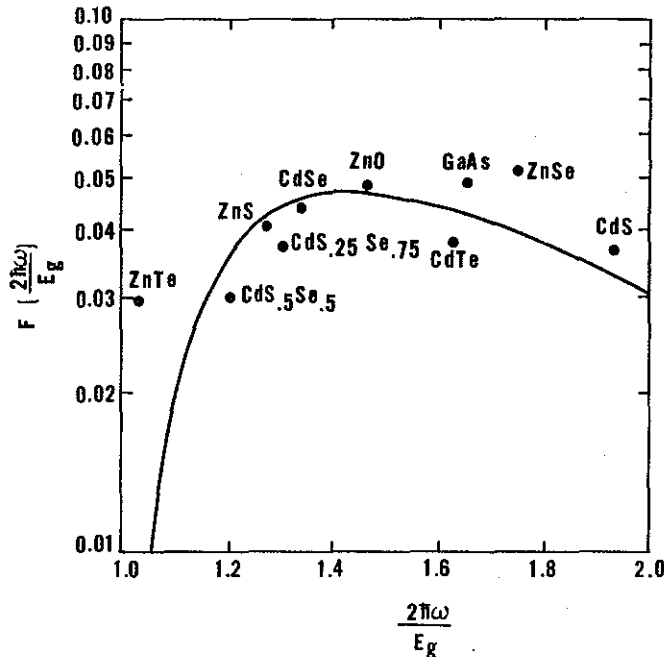


Figure 12. The solid line is the two-parabolic band prediction for the function  $F$  plotted as a function of  $2\hbar\omega/E_g$  using  $K=3100$  in Eq. 21. The data are scaled according to Eq. 21 are from Ref. [12, 62]. Figure reproduced from Ref. [62].

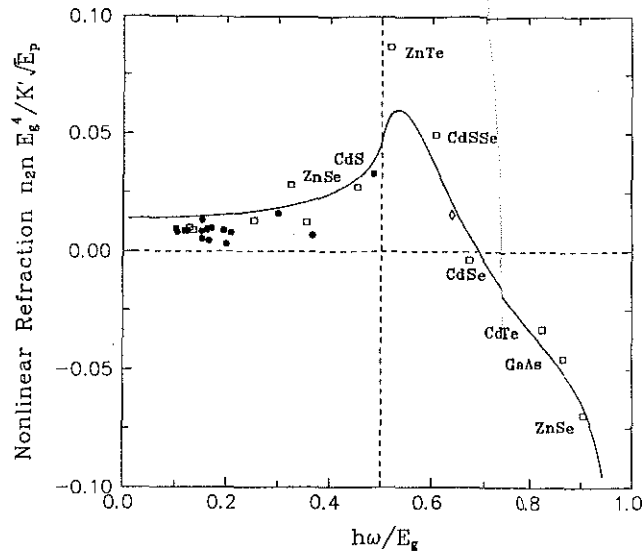


Figure 13. A plot of  $n_2$  data scaled according to Eq. 22. The circles are measurements in [40], the diamond is from [61], and the squares are our Z-scan measurements [19]. We have labeled the semiconductor data. The solid line is the function  $G(\hbar\omega/E_g)$  derived here for a two band model of a semiconductor using the 2PA data for the fit to the constant  $K'$ .

turns on, and then decreases, reaching negative values as  $\hbar\omega$  approaches the band edge. This curve is reminiscent of the behavior of the linear index in a solid which has its peak value at the band edge, where linear absorption turns on, and then rapidly turning down toward smaller values as  $\hbar\omega$  increases. Just as the linear index  $n$  is related to the linear absorption through Kramers-Kronig relations, so the nonlinear index is related to the nonlinear absorption. These nonlinear Kramers-Kronig relations are discussed in more detail in Refs. [18-21].

We find that the general trends in the data displayed in Figs. 12 and 13 are well described using the simplest possible band structure, i.e. two-parabolic bands. The solid line in Fig. 12 comes from a calculation of the transition rate for 2PA using such a band structure. Performing a Kramers-Kronig transformation on the nonlinear absorption calculated using this band structure gives the solid line of Fig. 13. While there are deviations from these curves of up to factors of 3, in general there is surprisingly good agreement considering the range of materials and differences in band-gap energies (from 0.2 to 10 eV). Using the calculated spectral responses, we can compare the range of values of  $\beta$  and  $n_2$  for the different materials studied by replotting the scaled data on a log-log plot versus  $E_g$  as in Figs. 14 and 15 (i.e. dividing out the respective theoretical frequency dependences of the nonlinearities). This shows the  $E_g^{-3}$  dependence of 2PA in Fig. 14 and the  $E_g^{-4}$  dependence of  $n_2$  in Fig. 15, revealing more than four orders-of-magnitude change in  $n_2$ .

After having separated the contributions of "fast" (i.e.  $\beta$  and  $n_2$ ) and "slow" (i.e.  $\sigma_r$ ) we can compare theoretical results for the free-carrier nonlinear refraction with experiment. As long as the

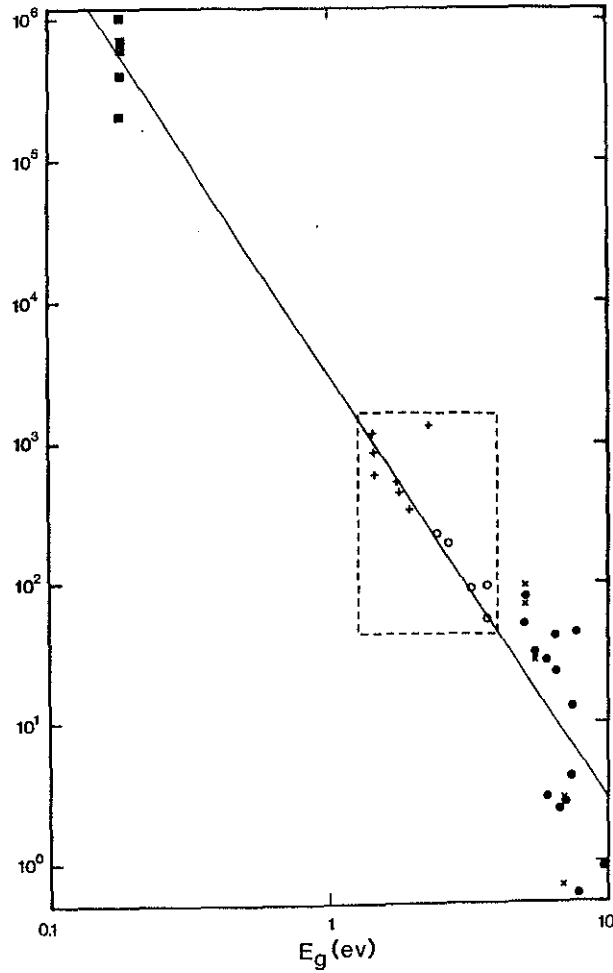


Figure 14. A log-log plot of the scaled 2PA coefficient  $\beta$  as a function of the bandgap energy  $E_g$  (in eV). The data are scaled from Eq. 21 as  $\beta^e n^2 / \sqrt{E_p} F$ . The straight line is a fit to the data within the dashed box from Ref. [62] for a line of fixed slope -3. The data to the right of the box are taken from Ref. [59] using the third (X's) and fourth (closed circles) harmonics of 1.06  $\mu\text{m}$  picosecond pulses. The data to the left of the box (closed squares) are taken from Ref. [60] using 10  $\mu\text{m}$  nanosecond pulses, which carefully accounted for free-carrier absorption. Figure reproduced from Ref. [64].

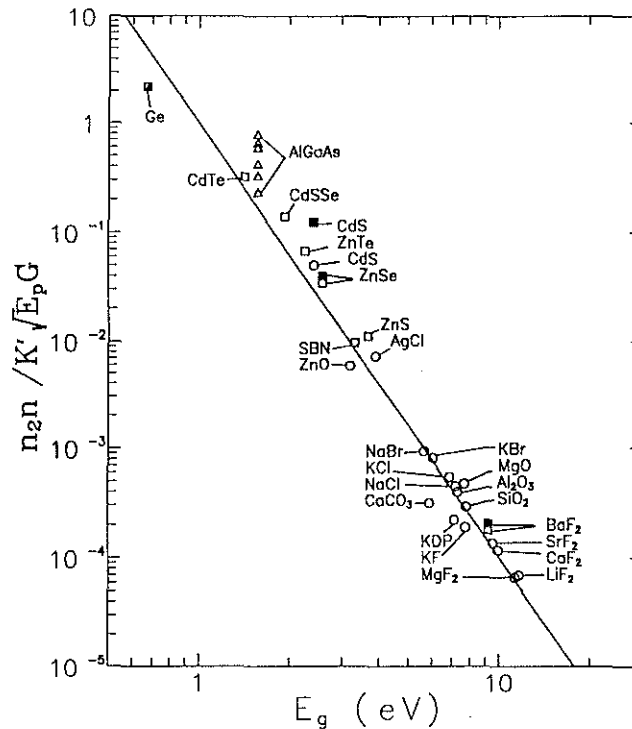


Figure 15. A log-log plot of scaled  $n_2$  data as a function of  $E_g$ . The data are scaled from Eq. 22 as  $n_2 n / K' \sqrt{E_p} G$ . The data (circles) are taken from Ref. [40] using nearly degenerate three-wave mixing, (squares) are Z-scan measurements from Ref. [19] (solid squares at  $0.532 \mu\text{m}$  open squares at  $1.06 \mu\text{m}$  and half shaded square at  $10.6 \mu\text{m}$ ), and the AlGaAs data (triangles) are taken from Ref. [63]. These data are now scaled by the dispersion function  $G$ . The solid straight line has a slope of  $-4$ .

photogenerated carriers thermalize extremely rapidly with the lattice,  $\sigma$  and  $\sigma_r$  are independent of their generation mechanism. The so-called Drude band-blocking theory of the frequency dependence of these carrier nonlinearities appears to describe experiments reasonably accurately under a variety of conditions such that the spectral dependences are known.[36-38] Reference 25 gives a detailed comparison of different theories with experiments on semiconductors.

## V. Conclusion

While we have only explicitly shown data for ZnSe, data obtained for other materials looks remarkably similar. For example, Fig. 16 shows Z-scan data for BaF<sub>2</sub> at an input wavelength of 266 nm where the material is a two-photon absorber ( $E_g \approx 9.2 \text{ eV}$ ). This figure is to be compared with Fig. 5 for ZnSe. The deviation of the fit for negative Z is due to a linear background (i.e. independent of I) caused by surface curvature. Such background effects become more pronounced at

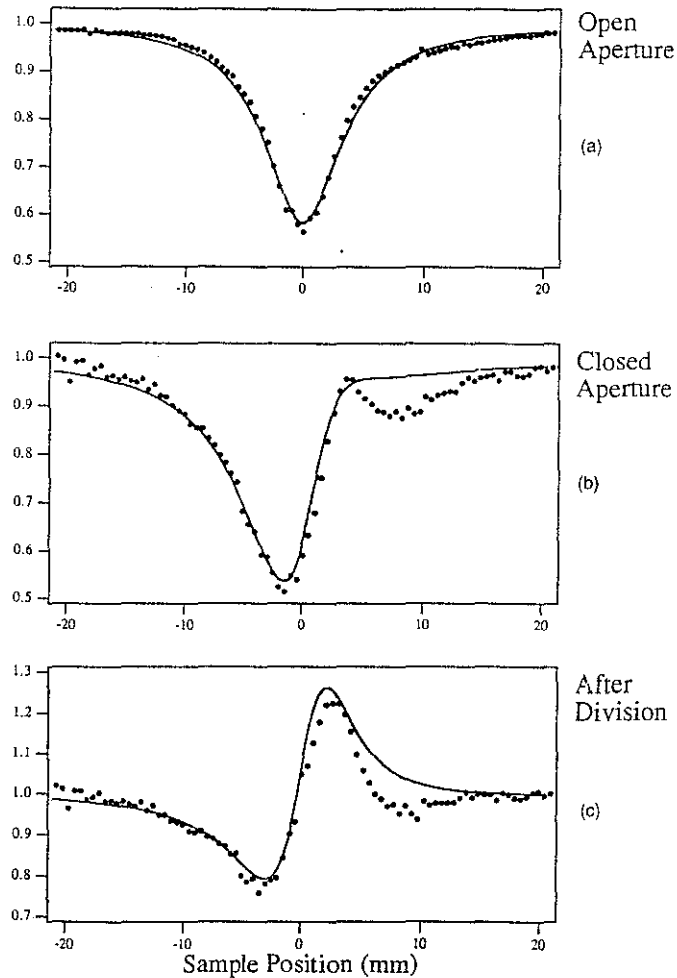
BaF<sub>2</sub> 266nm Z-Scans

Figure 16. Normalized Z-scan transmittance of BaF<sub>2</sub> measured using picosecond pulses at  $\lambda=266$  nm with  $I_0=72$  GW/cm<sup>2</sup>. (a) Open aperture data and fit (solid line) (b) 40% aperture data and fit (solid line) and (c) The result of the division of the Z-scans of (a) and (b).

shorter wavelengths. We find for BaF<sub>2</sub> at 266 nm, with the light propagating in the [100] direction and the field parallel to [010],  $\beta \approx 0.06$  cm/GW, and  $n_2 \approx +3.1 \times 10^{-16}$  cm<sup>2</sup>/W ( $+1.1 \times 10^{-13}$  esu) while the anisotropy in this material is large (eg. 30% change in  $n_2$  with orientation). While a thorough study at this wavelength has not been performed, we expect the free-carrier effects at this irradiance and wavelength are small. This is due to both the small magnitude of  $\beta$  and the smaller expected free-carrier cross sections at short wavelengths.

In order to extract the data needed to plot Figures 12, 13, 14 and 15, a clear understanding of the nonlinearities involved was necessary. In the final analysis these figures reveal relatively simple

trends and scaling rules. We have found that a simple 2-parabolic band model for semiconductors describes semiconductor data well and even appears to work for wide-gap dielectric materials.

The examples given here demonstrate the importance of measuring materials nonlinearities using different techniques and/or as functions of several parameters including pulsewidth and wavelength. For example had we only measured nonlinear refraction in ZnSe at one pulsewidth we could not have determined whether the response was due to a bound electronic  $n_2$  or to linearly generated free-carrier refraction. Additionally, the nonlinear refraction in ZnSe coming from the two-photon absorption generated carriers, depending on the irradiance range of the experiment, could be mistaken for a larger third-order response (i.e. the fifth-order response may not be recognized without analyzing data over an extended range of irradiance levels). In turn, when analyzing data from different materials in an attempt to discover scaling rules, trends could easily be masked if the nonlinearities were not properly separated.

The wavelength dependence is not only of importance to determine nonlinear mechanisms, but it can be crucial in determining whether a material is promising for a given application. As seen in Fig. 13,  $n_2$  has a zero near  $3/4 E_g$ . If a measurement were made near this wavelength, the material could be labeled useless for applications involving large  $n_2$ 's independent of how large the peak  $n_2$  is (see Fig. 13). While the wavelength dependence of the nonlinearities in these inorganic materials as shown in Figs. 12 and 13 is relatively simple, molecular (organic) crystals can be expected to have considerably more structure, for example several wavelength separated 2PA peaks. It is hoped that the knowledge gained in understanding the nonlinear response of inorganic materials will be helpful in unraveling the response of organics.

## VII. Acknowledgement

We gratefully acknowledge the support of the National Science Foundation grant ECS#9120590, the Defense Advanced Research Projects Agency, and the Night Vision and Electro-Optics Directorate. The work presented in this paper represents many years of effort involving many former and current students as well as post-doctoral fellows. We thank all those involved and acknowledge their contributions through the various referenced publications. We explicitly thank Edesly J. Canto-Said, J. Richard DeSalvo, David C. Hutchings, M.J. Soileau, Hermann Vanherzeele, Tai H. Wei, Milton A. Woodall, and Yuen-Yen Wu for their many contributions.

## REFERENCES:

- [1] M. J. Weber, D. Milam, and W. L. Smith, "Nonlinear refractive index of glasses and crystals", *Opt. Eng.*, 17, 463 (1978).
- [2] M. J. Moran, C. Y. She, and R. L. Carman, "Interferometric measurements of nonlinear refractive-index coefficient relative to  $CS_2$  in laser-system-related materials", *IEEE J. Quantum Electron.*, QE-11, 259 (1975).

- [3] R.K. Jain and M.B. Klein, "Degenerate Four-Wave Mixing in Semiconductors", pp. 307-415, in *Optical Phase Conjugation*, ed. R. A. Fisher, Academic Press, N.Y. 1983.
- [4] R. Adair, L. L. Chase, and S. A. Payne, "Nonlinear refractive index measurement of glasses using three-wave frequency mixing", *J. Opt. Soc. Am. B*, **4**, 875 (1987).
- [5] A. Owyong, "Ellipse rotations studies in laser host materials", *IEEE J. Quantum Electron.*, **QE-9**, 1064 (1973).
- [6] W. E. Williams, M. J. Soileau, and E. W. Van Stryland, "Optical Switching and  $n_2$  Measurements in  $CS_2$ ", *Opt. Commun.*, **50**, 256 (1984).
- [7] W. E. Williams, M. J. Soileau, and E. W. Van Stryland, "Simple direct measurement of  $n_2$ ", in *Proc. 15th Annu. Symp. Opt. Materials for High Power Lasers*, Boulder, CO, 1983.
- [8] M. Bertolotti, A. Ferrari, C. Sibilia, G. Suber, D. Apostol and P. Jani, "Photothermal Deflection Technique for Measuring Thermal Nonlinearities in Glasses", *Appl. Phys.*, **27**, 1811 (1988).
- [9] F. Kajzar and J. Messier, "Cubic Effects in Polydiacetylene Solutions and Thin Films", in *Nonlinear Optical Properties of Organic Molecules and Crystals*, eds. D.S. Chemla and J. Zyss, Vol. 2, pp. 51-83, Academic Press, Orlando, 1987.
- [10] M. Sheik-Bahae, A. A. Said, and E. W. Van Stryland, "High sensitivity, single beam  $n_2$  measurement", *Opt. Lett.*, **14**, 955-957 (1989).
- [11] M. Sheik-Bahae, A. A. Said, T. H. Wei, D. J. Hagan, and E. W. Van Stryland, "Sensitive measurement of optical nonlinearities using a single beam", *IEEE J. Quantum Electron.*, **QE-26**, 760-769 (1990).
- [12] E. W. Van Stryland, H. Vanherzeele, M. A. Woodall, M. J. Soileau, A. L. Smirl, S. Guha, and T. F. Boggess, "Two photon absorption, nonlinear refraction, and optical limiting in semiconductors", *Opt. Eng.*, **24**, 613 (1985).
- [13] M. Bass, E.W. Van Stryland, and A.F. Stewart, "Laser Calorimetric Measurement of Two-Photon Absorption", *Appl. Phys. Lett.* **34**, 142 (1979).
- [14] Y. Bae, J.J. Song, and Y.B. Kim, "Photoacoustic Study of Two-Photon Absorption in Hexagonal  $ZnS$ ", *J. Appl. Phys.*, **53**, 615 (1982). also see, E.W. Van Stryland, and M.A. Woodall, "Photoacoustic Measurement of Nonlinear Absorption in Solids," in *Laser Induced Damage in Optical Materials*, NBS Special Publication 620, 50 (1980).
- [15] for example see; *Picosecond Phenomena*, eds. C.V. Shank, E.P. Ippen, and S.L. Shapiro, Springer Verlag, 1978.

- [16] A. E. Kaplan, "External Self-Focusing of Light by a Nonlinear Lens", *Radiophys. Quantum Electron.*, 12, 692 (1969).
- [17] S. A. Akhmanov, R. V. Khokhlov, and A. P. Sukhorukov, "Self-Focusing, Self-Defocusing, and Self-Modulation of Laser Beams," in *Laser Handbook*, F. T. Arecchi and E. O. Shultz-Dubois, eds. (North-Holland, Amsterdam, 1972), vol. 2 1151-1228.
- [18] M. Sheik-Bahae, D. J. Hagan, and E. W. Van Stryland, "Dispersion and Band-Gap Scaling of the Electronic Kerr Effect in Solids Associated with Two-Photon Absorption", *Phys. Rev. Lett.*, 65 96-99 (1990).
- [19] M. Sheik-Bahae, D. Hutchings, D. J. Hagan, and E. W. Van Stryland, "Dispersion of Bound Electronic Nonlinear Refraction in Solids", *IEEE J. Quantum Electron.*, 27, 1296 (1991).
- [20] D.C. Hutchings, M. Sheik-Bahae, D.J. Hagan, and E.W. Van Stryland, "Kramers-Kronig Relations in Nonlinear Optics", *Optical and Quantum Electronics*, 24, 1-30 (1992).
- [21] F. Bassani and S. Scandolo, "Dispersion Relations in Nonlinear Optics", *Phys. Rev. B*44, 8446-8453 (1991).
- [22] see for example, Y.R. Shen, *The Principles of Nonlinear Optics*, John Wiley and Sons, New York, 1984.
- [23] T. H. Wei, D. J. Hagan, E. W. Van Stryland, J. W. Perry, and D. R. Coulter, "Direct Measurements of Nonlinear Absorption and Refraction in Solutions of Pthalocyanines", *Appl. Phys. B*54, 46 (1992).
- [24] T.F. Boggess, S.C. Moss, I.W. Boyd, and A.L. Smirl, "Nonlinear Optical Energy Regulation by Nonlinear Refraction and Absorption in Silicon", *Opt. Lett.* 9, 291-293, (1984).
- [25] A. A. Said, M. Sheik-Bahae, D.J. Hagan, T. H. Wei, J. Wang, J. Young, and E. W. Van Stryland, "Determination of Bound-Electronic and Free-Carrier Nonlinearities in ZnSe, GaAs, CdTe, and ZnTe", *J. Opt. Soc. Am. B*, 9, 405 (1992).
- [26] see for example, Kosar, in *Light-Sensitive Systems*, J. Wiley and Sons, Inc., N.Y., 1965. also see, D.R. Bosomworth and H.J. Gerritsen, "Thick Holograms in Photochromic Materials", *Appl. Opt.* 7, 95 (1968).
- [27] Nastaran Mansour, Kamjou Mansour, E.W. Van Stryland, and M.J. Soileau, "Diffusion of Color Centers Generated by Two-Photon-Absorption at 532nm in Cubic Zirconia", *Journal of Applied Physics* 67, 1475-1477 (1989).
- [28] J. H. Bechtel, and W. L. Smith, "Two-photon absorption in semiconductors with picosecond pulses", *Phys. Rev. B*13, 3515 (1976).

- [56] Ma Hai-Ming, "Self-transitions of picosecond light pulses in GaAs", in Chinese, Chinese Journal of Phys., 38, 153 (1989).
- [57] A.A. Bugaev, T.Yu. Dunaeva and V.A. Lukoshkin, "Influence of Nonlinear Refraction, Absorption by Free Carriers, and Multiple Reflection on the Determination of the Two-Photon Absorption Coefficient of GaAs", Sov. Phys. Solid State 31, 2031-2034 (1990).
- [58] J.S. Aitchison, M.K. Oliver, E. Kapon, E. Colas and P.W.E. Smith, "Role of Two-Photon Absorption in Ultrafast Semiconductor Optical Switching Devices", Appl. Phys. Lett. 56, 1305-1307 (1990).
- [59] P. Liu, W.L. Smith, H. Lotem, J.H. Bechtel, and N. Bloembergen, "Absolute Two-Photon Absorption Coefficients at 355 and 266 nm", Phys. Rev. B 17, 4620 (1978).
- [60] J. Dempsey, J. Smith, G.D. Holah, and A. Miller, "Nonlinear Absorption and Pulse-Shaping in InSb", Opt. Commun. 26, 265 (1978); A.M. Johnson, C.R. Pidgeon, and J. Dempsey, "Frequency Dependence of Two-Photon Absorption in InSb and HgCdTe", Phys. Rev. B 22, 825 (1980); C.R. Pidgeon, B.S. Wherrett, A.M. Johnson, J. Dempsey, and A. Miller, "Two-Photon Absorption in Zinc-Blende Semiconductors", Phys. Rev. Lett. 42, 785 (1979).
- [61] I.N. Ross, W.T. Toner, C.J. Hooker, J.R.M. Barr, and I. Coffey, "Nonlinear Properties of Silica and Air for Picosecond Ultraviolet Pulses", J. Modern Opt. 37, 555-573 (1990).
- [62] Eric W. Van Stryland, M.A. Woodall, H. Vanherzeele, and M.J. Soileau, "Energy Band-Gap Dependence of Two-Photon Absorption", Opt. Lett. 10, 490 (1985).
- [63] M.J. LaGasse, K.K. Anderson, C.A. Wang, H.A. Haus, and J.G. Fujimoto, "Femtosecond Measurements of the Nonresonant Nonlinear Index of in AlGaAs", Appl. Phys. Lett. 56, 417-419 (1990).
- [64] E.W. Van Stryland, Y.Y. Wu, D.J. Hagan, M.J. Soileau, and Kamjou Mansour, "Optical Limiting with Semiconductors", J. Opt. Soc. Am. B 5, 1980-1989 (1988).



**ERIC W. VAN STRYLAND** received the Ph.D. degree in physics in 1976, from the University of Arizona, Optical Sciences Center, Tucson, AZ, where he worked on optical coherent transients. He worked in the areas of femtosecond pulse production, multiphoton absorption in solids, and laser-induced damage at the Center for Laser Studies at the University of Southern California. He joined the physics department at the University of North Texas in 1978 and was instrumental in forming the Center for Applied Quantum Electronics. In 1987 he joined the newly formed Center for Research in Electro-Optics and Lasers at the University of Central Florida where he is a Professor of Physics and Electrical and Computer Engineering. He has been funded by NSF for the past fifteen years as well as performing funded research for the DoD. His current research interests are in the characterization of the nonlinear optical properties of materials and their temporal response as well as the applications of these nonlinear materials properties for sensor protection, beam control, switching etc.



**Mansoor Sheik-Bahae (M'87)** was born in Isfahan, Iran in 1956. He received the B.S. and M.S. degrees in electrical engineering from Catholic University of America, Washington D.C., in 1980 and 1982 respectively and Ph.D. degree in electro-physics from State University of New York (SUNY) at Buffalo, N.Y. in 1987. He then joined the Center for Research and Education in Optics and Lasers (CREOL) at the University of Central Florida, Orlando, where he is now an Associate Research Professor in the area of nonlinear optics and ultrafast phenomena. His research interests include experimental and theoretical study of nonlinear optical processes in bulk semiconductors and semiconductor diode lasers. He has also been involved in the development and characterization of the femtosecond solid-state and picosecond CO<sub>2</sub> laser systems.

Dr. Sheik-Bahae is a member of the Optical Society of America and IEEE Lasers and Electro-Optics Society (LEOS).



Ali A. Said was born in Lebanon in 1959. He received the B.S. degree in physics and mathematics from Southeastern Oklahoma State University in 1982, and the M.S. and Ph.D. degrees from the University of North Texas in 1984 and 1991, respectively. His research for the Ph.D. degree was conducted at the Center for Research and Education in Optics and Lasers (CREOL) at the University of Central Florida.

He is currently a research scientist at CREOL and his current research activities include measurement of optical nonlinearities in semiconductors, dielectrics, and organic liquids and thin films, and the application of nonlinear refraction and absorption to optical limiting.

Dr. Said is a member of the Optical Society of America, and the Society of Photo-optical Instrumentation Engineers.



**David J. Hagan**

Dr. Hagan was born in Edinburgh, Scotland in 1959. He received the degrees of BSc and PhD in physics from Heriot-Watt University, Edinburgh, in 1985, where he worked on infrared nonlinear optical phase conjugation and optical bistability. He joined the faculty at CREOL in 1987 after two years at North Texas State University where he performed research on self-protecting optical limiters. Dr. Hagan's primary research interest is in characterization of nonlinear optical materials, including bulk inorganics, organic solutions, and microstructures. He is a member of IEEE and the Optical Society of America.

